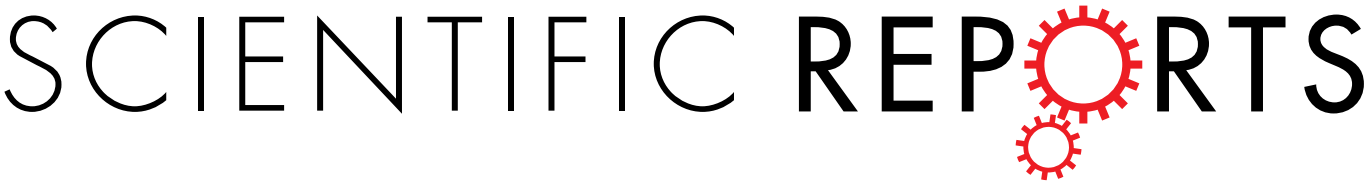

OPEN

Action potential initiation in a two-compartment model of pyramidal neuron mediated by dendritic Ca^{2+} spike

Received: 19 December 2016
Accepted: 02 March 2017
Published: 03 April 2017

Guosheng Yi, Jiang Wang, Xile Wei & Bin Deng

Dendritic Ca^{2+} spike endows cortical pyramidal cell with powerful ability of synaptic integration, which is critical for neuronal computation. Here we propose a two-compartment conductance-based model to investigate how the Ca^{2+} activity of apical dendrite participates in the action potential (AP) initiation to affect the firing properties of pyramidal neurons. We have shown that the apical input with sufficient intensity triggers a dendritic Ca^{2+} spike, which significantly boosts dendritic inputs as it propagates to soma. Such event instantaneously shifts the limit cycle attractor of the neuron and results in a burst of APs, which makes its firing rate reach a plateau steady-state level. Delivering current to two chambers simultaneously increases the level of neuronal excitability and decreases the threshold of input-output relation. Here the back-propagating APs facilitate the initiation of dendritic Ca^{2+} spike and evoke BAC firing. These findings indicate that the proposed model is capable of reproducing *in vitro* experimental observations. By determining spike initiating dynamics, we have provided a fundamental link between dendritic Ca^{2+} spike and output APs, which could contribute to mechanically interpreting how dendritic Ca^{2+} activity participates in the simple computations of pyramidal neuron.

Pyramidal neurons are common cell types found in the cerebral cortex and hippocampus of mammalian brain[1–3]. Their structures are characterized by a pyramidal shaped soma and extended apical and basal dendritic trees. This kind of nerve cells have powerful capability of processing information, which could effectively and precisely transform incoming signals into specific patterns of action potential (AP) output. During this procedure, their dendrites play a particularly vital role, since they are the predominant receiving sites for synaptic signals[1,4–8]. The vast branches of dendritic tree endow a pyramidal cell with distinctive morphological feature, which disperse the primary input locations. It is known that APs usually occur in the initial segment of the axon. Due to such spatial arrangement, the apical dendrites have to deliver input signals to the site of AP initiation. Their function is not solely to receive information from connected input cells and transmit it to the axon. Each dendritic branch is also a basic signalling unit for integrating synaptic inputs[4,6–11], which determines how the receiving signals propagate to the axon. Such nonlinear integration operated by dendrites has a profound influence on neuronal and cortical computation[1,2,4–10].

The dendrites of pyramidal cells rely on their intrinsic nonlinearities, including voltage-gated channels and complex morphology, to integrate synaptic signals[4–11]. The active ionic channels in their apical dendrites are particularly important in synaptic integration. A common channel is the voltage-dependent Ca^{2+} current that flows into the cell[1,4–7,12–14]. The activation of its conductance could cause a threshold-dependent, all-or-none regenerative response in dendrites, which is often referred to as dendritic Ca^{2+} spike[4,7,11,14–17]. The existence of active Ca^{2+} channel in apical dendrites make pyramidal neurons operate in either global or two-stage integration mode[18,19]. For simple global integration mode, input signals directly contribute to AP output by triggering excitatory post-synaptic potentials (EPSPs) that spread to the AP initiation zone. In latter integration mode, the synaptic input directly activates the Ca^{2+} channel in dendrites and triggers dendritic spikes[7,14–17,20], which propagates forward to the axon where the global integration occurs[18,19]. Such integration lies at the heart of neural computation, which is tightly related to coincidence detection[1,16,21,22], orientation tuning[22], binding of synaptic signals from brain areas[23],

School of Electrical and Information Engineering, Tianjin University, Tianjin 300072, China. Correspondence and requests for materials should be addressed to X.L.W. (email: xilewei@tju.edu.cn)

and enhancing stimulus selectivity[24]. Understanding how it participates in AP output is therefore fundamental to understanding how relevant circuits function in cortical computation of mammalian brain.

Earlier studies have extensively explored the dendritic Ca^{2+} activities and their effects on neuronal firing behaviors with *in vitro* approaches. It is found that the synaptic inputs at different sites of dendrite[16,17,25], the back-propagating APs[17,26,27], and the local NMDA spikes[7,28,29] are all important determinants for activating Ca^{2+} conductance and triggering dendritic Ca^{2+} spike. This regenerative event at apical dendrites can boost distal synaptic inputs and enhance synaptic efficacy, which is hypothesized as the main biological mechanism for propagating synaptic inputs at the distal tuft to the soma of layer 5 pyramidal neurons[15–17,28]. It is usually characterized by a steep change followed by a plateau in the subthreshold input-output transformations conferred by dendrites. Further, the additional inward current associated with Ca^{2+} spike provides a strong local depolarization in dendritic membrane, which can enhance the somatic/axonal AP outputs. In particular, it can significantly increase the gain of input-output relation of pyramidal neuron, which triggers a burst of APs in the soma/axon and switches the firing mode of the cell to bursting[23,26,30–32]. However, it is still not well understood how dendritic Ca^{2+} spike participates in AP initiation to influence the somatic/axonal output.

In addition to above *in vitro* observations, there are also modeling studies that focus on the dendritic Ca^{2+} activity[21,33–37]. Most of them use biophysically realistic neurons that are modeled in NEURON or GENESIS to understand the mechanism underlying the generation and propagation of dendritic Ca^{2+} spike. Such complex multi-compartment models are not sufficiently simple to allow one to uncover the dynamical or biophysical basis for AP initiation related to dendritic Ca^{2+} activity. There are also studies that use two compartments to model pyramidal neurons with dendritic Ca^{2+} channel. Such simple point-neuron models have been adopted to study their firing patterns[38–40], spike-timing predictions[41], spike timing-dependent plasticity[42], and spike-frequency adaptation[43]. However, it has attracted little attention about the somatic/axonal AP initiation associated with dendritic Ca^{2+} spike. Further, Larkum *et al.*[26] have used a two-compartment integrate-and-fire (IF) model to reproduce the gain modulation of pyramidal cell induced by top-down dendritic Ca^{2+} spike. However, in IF model an AP is explicitly generated when its membrane voltage reaches a predefined threshold[44]. That is, the IF model is unable to reproduce how inward and outward ionic currents interact at the subthreshold potentials to initiate AP. Therefore, it is still largely unknown that how dendritic Ca^{2+} spike affects the AP initiation of individual pyramidal cells.

Here we develop a five-dimensional (5D) two-compartment model (as shown in Fig. 1a) by introducing Ca^{2+} current into the passive dendrite of a reduced Pinsky-Rinzel (PR) model[45,46]. Contrary to IF model, the generation of APs in our model implicitly results from the dynamical interactions of inward Na^+ and outward K^+ currents at the subthreshold voltages[45–47]. With this model, we have systematically investigated the firing behaviors of the pyramidal neuron with passive and active dendrite to the input current injected at different sites of the neuron. The dynamical basis for relevant AP initiation is determined with phase plane and bifurcation analysis. Our simulations indicate that the proposed model here is able to reproduce a variety of *in vitro* experimental observations of pyramidal neurons, which is also amenable to both dynamical analysis and efficient simulation.

Results

Somatic input is unable to trigger dendritic Ca^{2+} spike in the absence of dendritic input. We first investigate the spiking properties of the 5D model neuron to somatic input I_S. The current I_D injected at dendritic chamber is absent, i.e., $I_D = 0\ \mu A/cm^2$. Figure 1b–e give the input-output relation and corresponding dynamical basis of AP initiation in the case of $\bar{g}_{Ca} = 40\ mS/cm^2$. We find that the neuron is unable to generate APs when $I_S < 33.9\ \mu A/cm^2$ (Fig. 1b and d). At these small values of I_S, the neuron exist in quiescent state and its somatic membrane potential V_S is eventually stabilized at a subthreshold voltage. With $I_S \geq 33.9\ \mu A/cm^2$, the neuron generates repetitive APs. In this case, the average firing rate f_S increases with input I_S from 0 Hz. The relation between f_S and I_S (i.e., $f_S - I_S$ curve) is continuous (Fig. 1d).

Figure 1c illustrates the dynamical basis of AP initiation associated with the observed behaviors shown in Fig. 1b and d. With $I_S < 33.9\ \mu A/cm^2$, the V_S- and w-nullclines intersect at three points in $w - V_S$ phase plane (left panel, Fig. 1c). Since the leftmost intersection is a stable node, all of V_S trajectories converge to this equilibrium and the neuron does not fire APs. Increasing I_S shifts V_S-nullcline upwards, while does not alter the position of w-nullcline. In this case, the distance between stable node and unstable saddle decreases. With $I_S = 33.9\ \mu A/cm^2$, these two equilibriums coalesce and annihilate each other. At the same time, a stable limit cycle is generated in $w - V_S$ phase plane (Fig. 1c). Since the stable node corresponding to resting state no longer exists, V_S trajectory jumps to the limit cycle attractor and the neuron starts to fire tonic spikes. The transition from resting to repetitive spiking occurs through a saddle-node on invariant circle (SNIC) bifurcation of equilibrium (Fig. 1e), which corresponds to the continuous $f_S - I_S$ curve.

In the absence of I_D, the firing rate f_S of the model evoked by I_S does not change with the maximum conductance $\bar{g}_{Ca}$ of dendritic Ca^{2+} current (Fig. 1f). With $I_D = 0\ \mu A/cm^2$, there is no external driver activating Ca^{2+} conductance and thus dendritic Ca^{2+} spike is missing. Here I_S only activates the Na^+ channel in soma. Although the Na^+-APs can be back-propagated to dendrite, such bottom-up input is unable to drive V_D to reach the threshold voltage for activating Ca^{2+} current (Fig. 1g). Under these conditions, increasing $\bar{g}_{Ca}$ produces no effects on the spiking behaviors of the neuron to somatic input.

Apical input activates dendritic Ca^{2+} current and results in burst of somatic APs. In this section, we investigate how 5D model neuron responds to apical input injected at dendrite. Here somatic input I_S is absent, i.e., $I_S = 0\ \mu A/cm^2$. The firing behaviors of the model is determined with different values of $\bar{g}_{Ca}$, which are summarized in Fig. 2.

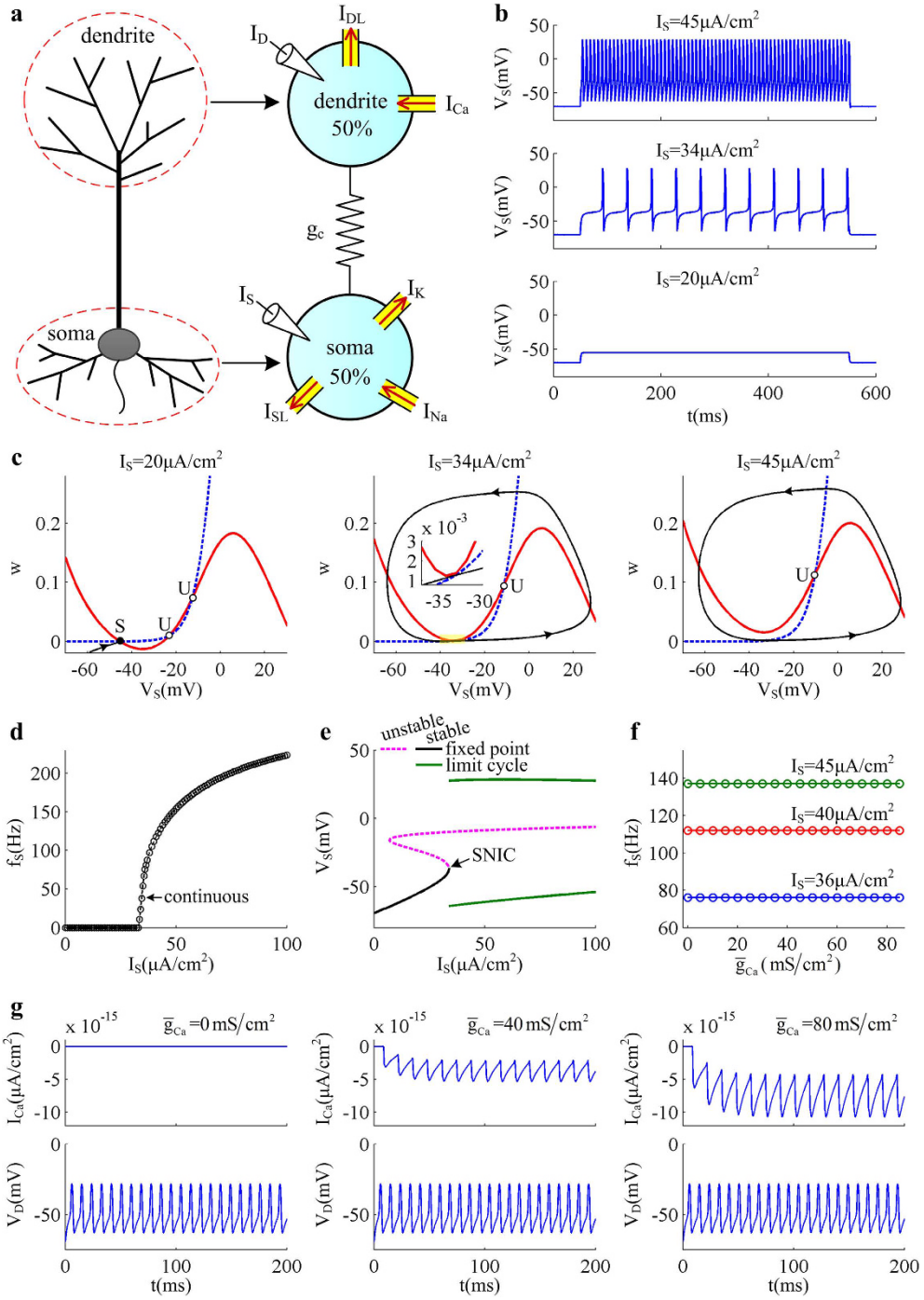

Figure 1. Input-output relation and relevant spike initiating dynamics evoked by somatic input. (**a**) 5D two-compartment model of the pyramidal neuron. One chamber represents the basal zone around soma, and the other one is apical dendrite. Two chambers are connected by an internal conductance g_c. The stimulus current can be independently injected into soma and dendrite. Red arrows in the right panel indicate the direction of relevant current flow. (**b**) Sample responses triggered by three values of I_S, which is indicated on the top of each panel. (**c**) Phase portraits in $w - V_S$ plane to subthreshold and suprathreshold I_S. Blue dotted line represents w-nullcline and red solid line is V_S-nullcline. They represent the states where corresponding variable neither increases nor decreases. Black solid line is a sample V_S trajectory, where arrows indicate the direction of its motion. 'S' indicates the intersection between two nullclines is stable and 'U' is unstable. **(d)** Relation between average firing rate f_S and somatic input I_S, i.e., $f_S - I_S$ curve. **(e)** Bifurcation diagram of the 5D model, here the bifurcation parameter is I_S. Vertical axis gives the somatic voltage V_S at the fixed point or at the max/min of limit cycle as input I_S is increased. **(f)** Relation between average firing rate f_S and Ca^{2+} conductance $\bar{g}_{Ca}$ (i.e., $f_S - \bar{g}_{Ca}$ curve) with three values of input I_S. **(g)** Time courses of dendritic Ca^{2+} current I_{Ca} and dendritic voltage V_D in the cases of $\bar{g}_{Ca} = 0\,mS/cm^2$, $40\,mS/cm^2$, and $80\,mS/cm^2$. Corresponding somatic injection is $I_S = 40\mu A/cm^2$. For **(b–g)**, the dendritic input is $I_D = 0\mu A/cm^2$.

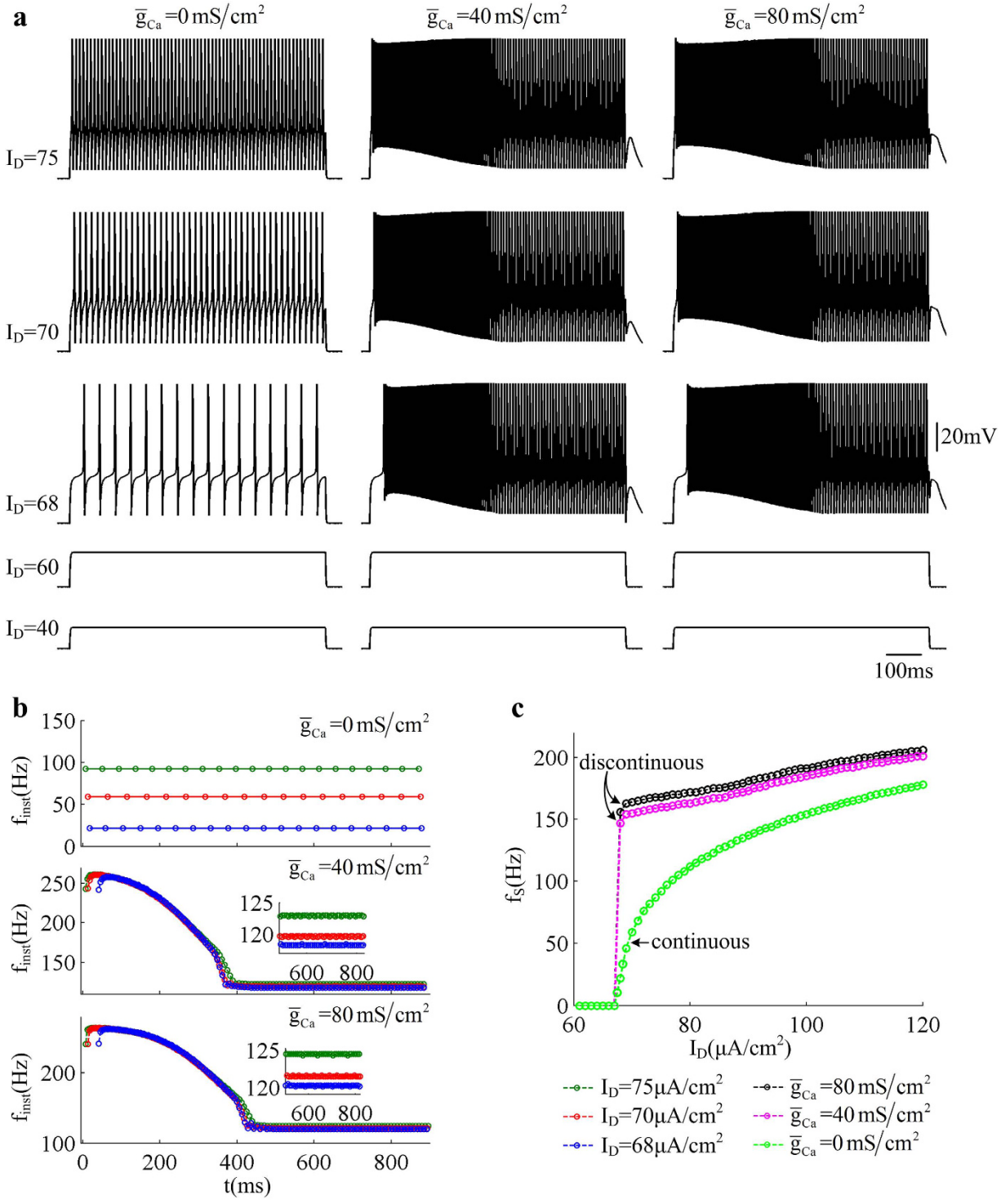

Figure 2. Firing properties evoked by dendritic input. (**a**) Sample responses of the 5D model triggered by apical input I_D in the cases of $\bar{g}_{Ca} = 0$ mS/cm^2, 40 mS/cm^2, and 80 mS/cm^2. I_D is in μA/cm^2, which is indicated on the left. **(b)** Instantaneous firing rate f_{inst} with three values of $\bar{g}_{Ca}$. Corresponding dendritic inputs are $I_D = 68$ μA/cm^2, 70 μA/cm^2, and 75 μA/cm^2. (**c**) Relation between average firing rate f_S and input I_D (i.e., $f_S - I_D$ curve) with three values of $\bar{g}_{Ca}$. Somatic injection is $I_S = 0$ μA/cm^2.

With $\bar{g}_{Ca} = 0$ mS/cm^2, the dendritic Ca^{2+} current is blocked and the dendrite becomes passive. In this case, the neuron exists in quiescent state with $I_D < 67.8$ μA/cm^2 and there are still no APs generated. Once I_D exceeds 67.8 μA/cm^2, repetitive APs are initiated in somatic chamber (left panel, Fig. 2a). The threshold of I_D here is much

larger than that of I_S directly injected to soma. This is because the dendritic compartment in the model serves as a current sink allowing only part of the input current to invade the soma. From Fig. 2c, one can find that the $f_S - I_D$ curve is continuous when blocking dendritic Ca^{2+} current, which indicates that the neuron is able to fire low-frequency APs to injected current I_D. As I_D is increased, the slope of $f_S - I_D$ curve (i.e., input-output gain) is obviously reduced. Further, the evoked spike trains are always repetitive and the instantaneous firing rate f_{inst} remains constant with time (top panel, Fig. 2b). The f_{inst} in our study is calculated based on the reciprocal of relevant ISI in each spike train.

With $\bar{g}_{Ca} = 40$ mS/cm^2 or 80 mS/cm^2, there is active Ca^{2+} current in dendritic chamber. We find that the threshold value of I_D for triggering somatic APs does not change with $\bar{g}_{Ca}$, which is still 67.8 μA/cm^2. However, the time course of the spike train is no longer repetitive (center and right panels, Fig. 2a). At the onset of I_D, the model generates a burst of high-frequency spikes, which then slowly transits to repetitive spiking with low frequency. From Fig. 2b, one can observe that the instantaneous firing rate f_{inst} first quickly increases to a peak value and then slowly decays to a lower plateau level. Under these conditions, the $f_S - I_D$ curve with $\bar{g}_{Ca} > 0$ mS/cm^2 is no longer continuous, and the neuron becomes unable to maintain low-frequency spiking. As shown in Fig. 2c, the average firing rate f_S immediately jumps to a high value once I_D reaches the threshold for triggering APs. After that, the slope of $f_S - I_D$ curve (i.e., input-output gain) with $\bar{g}_{Ca} = 40$ mS/cm^2 or 80 mS/cm^2 both changes little as I_D is increased. These simulations indicate that the activation of dendritic Ca^{2+} current boosts excitatory input I_D and facilitates the generation of somatic APs, i.e., an active dendritic integration occurs.

Dynamical basis for the burst of APs associated with dendritic Ca^{2+} spike. In previous section, we have determined the spiking properties of 5D model neuron stimulated by apical input I_D alone. Our next step is to uncover the AP initiating dynamics associated with these behaviors.

When blocking dendritic Ca^{2+} current (i.e., $\bar{g}_{Ca} = 0$ mS/cm^2), the dendrite becomes passive. Its membrane voltage V_D only oscillates repetitively along with V_S and there are no dendritic spikes evoked (left panels, Fig. 3a). Here the internal current I_{DS} between two chambers is also repetitive, which transmits depolarizing input I_D from dendrite to soma. Under these conditions, the intersection between V_S- and w-nullclines and corresponding limit cycle attractor both remain unchanged from one AP to the next (Fig. 3b). As a result, the neuron generates repetitive spike trains.

With $\bar{g}_{Ca} = 40$ mS/cm^2, the onset of apical input I_D depolarizes membrane voltage V_D and V_S. When V_D exceeds a threshold value, the Ca^{2+} conductance is activated and then a broader Ca^{2+} spike is initiated in the dendrite (right panels, Fig. 3a). When this event occurs, I_{Ca} first rapidly falls to a minimum value and then slowly rises to a steady-state plateau level. Note that the negative sign of I_{Ca} means this current is inward. Since Ca^{2+} flows into the dendritic cell, such Ca^{2+} spike evokes a prolonged obvious depolarization of dendritic membrane voltage. Under these conditions, there is an obviously depolarizing sink in internal current I_{DS}, which coincides with dendritic Ca^{2+} spike. That is, the presence of dendritic Ca^{2+} spike boosts apical input as it spreads to soma. Due to such active integration, a constant input of $I_D = 75$ μA/cm^2 is amplified to a non-periodic current I_{DS} with a maximum intensity around 146.3 μA/cm^2 to invade the soma. Such depolarizing internal current shifts V_S-nullcline upwards instantaneously in the first rapid phase of Ca^{2+} spike, and forces two nullclines to interact at an unstable fixed point (Fig. 3c). Then all of the V_S trajectories converge to limit cycle attractor, and the neuron generates initial APs. Before I_{Ca} reaches peak value, the amplitude of depolarizing I_{DS} continues to increase. It drives unstable fixed point upwards and the limit cycle attractor moves upwards accordingly, which makes firing rate f_{inst} further increase. In the second phase of dendritic Ca^{2+} spike, I_{Ca} slowly gets weak and the amplitude of depolarizing I_{DS} becomes to decrease. In this case, the unstable fixed point and relevant limit cycle attractor both moves downwards (Fig. 3c), which leads to a decay of firing rate f_{inst} to its steady-state plateau level. Therefore, the model generates a burst of somatic APs when dendritic Ca^{2+} spike is initiated. Once such local spike is evoked, the amplitude of dendritic voltage V_D and internal current I_{DS} with a specific value of $\bar{g}_{Ca}$ both varies little with apical input I_D. Then, the input-output gain with $\bar{g}_{Ca} = 40$ mS/cm^2 or 80 mS/cm^2 changes little in the observed range of I_D.

Figure 4 shows the AP initiating dynamics associated with the firing behaviors of the neuron as Ca^{2+} conductance $\bar{g}_{Ca}$ is increased from 0 mS/cm^2 to 90 mS/cm^2. Increasing $\bar{g}_{Ca}$ results in more somatic APs during the course of dendritic Ca^{2+} spike (Fig. 4a and b). It is known that the intensity of I_{Ca} is proportional to $\bar{g}_{Ca}$, and increasing its conductance extends the duration of dendritic Ca^{2+} spike (Fig. 4c). Then, the depolarizing current I_{DS} induced by dendritic spike becomes progressively more prominent with $\bar{g}_{Ca}$. Such stronger depolarizing current accelerates the spike initiation in somatic chamber, and drives neuron to fire more APs at a given value of I_D. Then, the average firing rate f_S increases as Ca^{2+} conductance is increased (Fig. 4d). However, varying $\bar{g}_{Ca}$ does not alter the kinetics or voltage-dependency of Ca^{2+} current. Then, the threshold of apical input I_D for activating dendritic Ca^{2+} channel or evoking somatic APs remains unchanged as $\bar{g}_{Ca}$ is increased (Fig. 4d). From Fig. 4e, one can find that blocking dendritic Ca^{2+} current results in a SNIC bifurcation of the equilibrium, which endows the neuron with a continuous $f_S - I_D$ curve (Fig. 2c). Introducing dendritic Ca^{2+} channel extends the stable limit cycle to the value of I_D below the bifurcation point of equilibrium, followed by unstable limit cycle. In this case, the equilibrium loses its stability via a saddle-node (SN) bifurcation, which corresponds to the transitions of resting to tonic spiking. When such kind of bifurcation occurs, the neuron fails to fire low-frequency APs[48], and its $f_S - I_D$ curve becomes discontinuous (Fig. 2c). Unlike equilibrium, the limit cycle transits from unstable to stable via saddle homoclinic orbit (SHO) bifurcation (Fig. 4e). As I_D is increased, the unstable limit cycle disappears via a subcritical SHO bifurcation, and the stable limit cycle appears via a supercritical SHO bifurcation. The presence of Ca^{2+} current in dendrite increases the dimension of the system, and makes the SHO bifurcations of limit cycle attractor occur at the value of I_D below SN bifurcation. What's more, the SHO bifurcation also occurs at different values of apical input as $\bar{g}_{Ca}$ is increased (Fig. 4e). All these modulations of firing behavior and corresponding

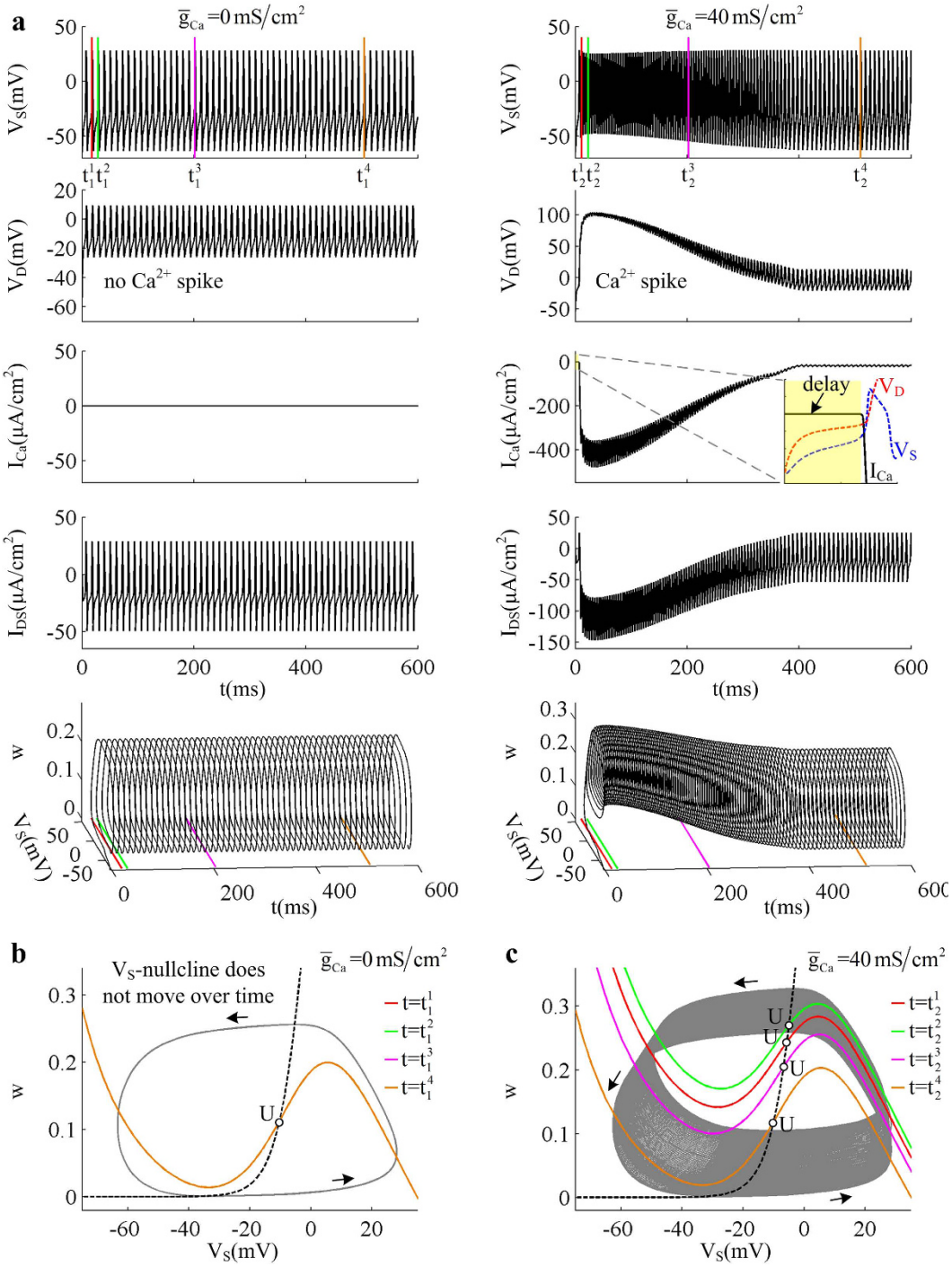

Figure 3. Spike initiating dynamics evoked by dendritic input. (**a**) Sample responses of the 5D model with $\bar{g}_{Ca} = 0$ mS/cm^2 and 40 mS/cm^2. Somatic voltage V_S, dendritic voltage V_D, dendritic Ca^{2+} current I_{Ca}, and internal current I_{DS} are plotted against time. The close-up shows that the Ca^{2+} conductance is activated when dendritic voltage V_D exceeds a threshold value. The sample response is also plotted in $w - V_S - t$ space (bottom panel). Color lines indicate the times at which the nullclines in **(b)** and **(c)** are calculated. Here dendritic input is $I_D = 75$ μA/cm^2. **(b)** Two-dimensional phase portraits in $w - V_S$ plane for $\bar{g}_{Ca} = 0$ mS/cm^2. **(c)** Phase portraits in $w - V_S$ plane for $\bar{g}_{Ca} = 40$ mS/cm^2. For **(b)** and **(c)**, the V_S- and w-nullclines are respectively calculated at four time points indicated by colored lines in (**a**). Black dotted lines represent w-nullclines, which are the same at different time points. The inverted N-shape lines with other colors are the V_S-nullcline at the corresponding time point indicated in **(a)**. With $\bar{g}_{Ca} = 0$ mS/cm^2, the V_S-nullcline does not move over time. Gray solid line is the sample V_S trajectory of the recorded spike trains, and black arrows indicate the direction of its motion. 'U' indicates unstable fixed point. Somatic injection is $I_S = 0$μA/cm^2.

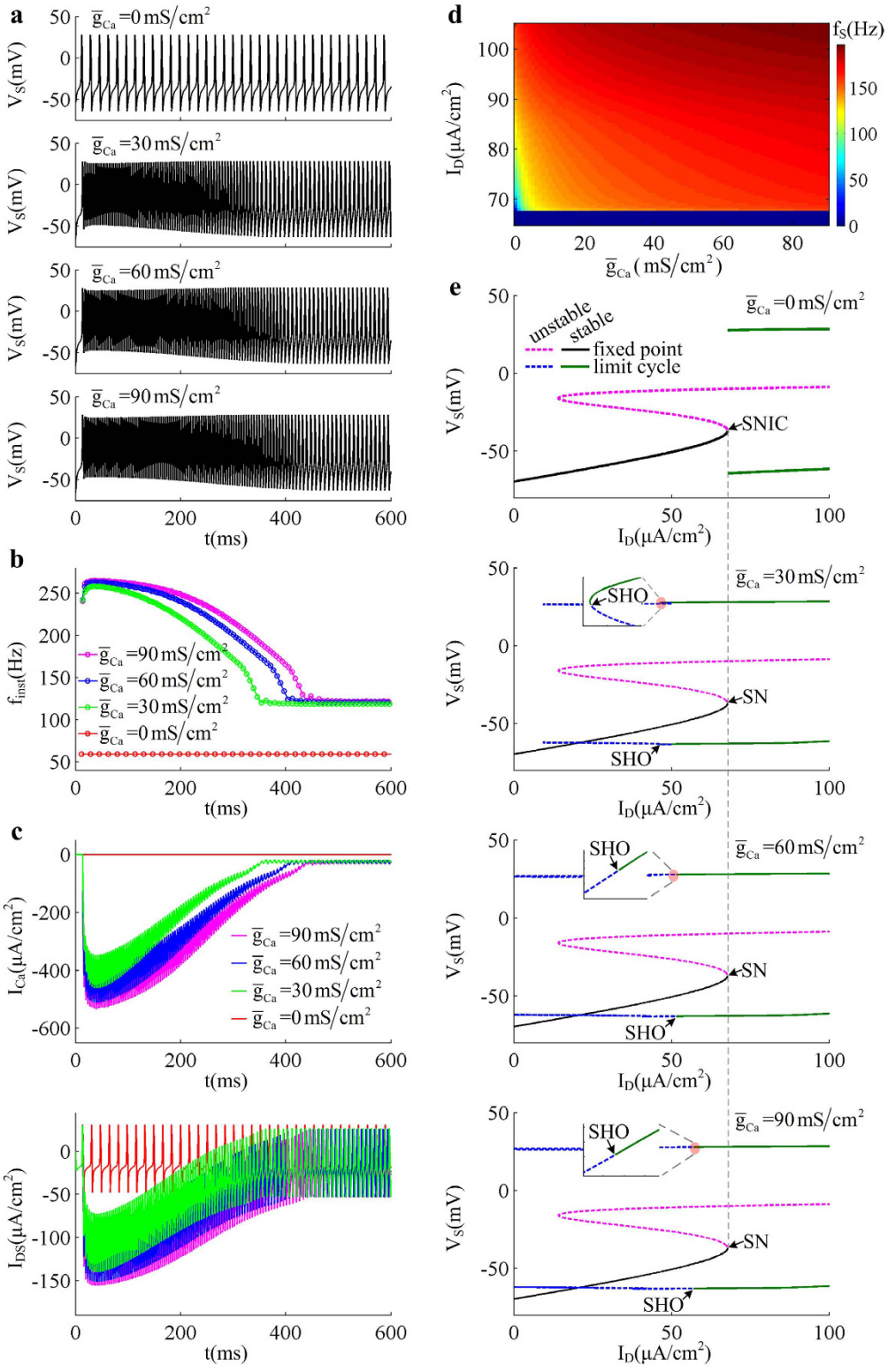

Figure 4. Effects of varying Ca^{2+} conductance on spike initiating dynamics evoked by dendritic input. (**a**) Spike train recorded in the soma of 5D model in the cases of $\bar{g}_{Ca} = 0$ mS/cm^2, 30 mS/cm^2, 60 mS/cm^2, and 90 mS/cm^2. (**b**) The instantaneous firing rate f_{inst} for each spike train. (**c**) Time courses of dendritic Ca^{2+} current I_{Ca} and corresponding internal current I_{DS} with each value of $\bar{g}_{Ca}$. For (**a**–**c**), the corresponding dendritic input is $I_D = 70$ μA/cm^2. (**d**) Average firing rate f_S is plotted against I_D and $\bar{g}_{Ca}$. (**e**) Bifurcation diagram with different values of $\bar{g}_{Ca}$. Here the bifurcation parameter is apical input I_D. Type of the bifurcation for equilibrium or limit cycle is indicated on each plot. Somatic input is $I_S = 0$ μA/cm^2.

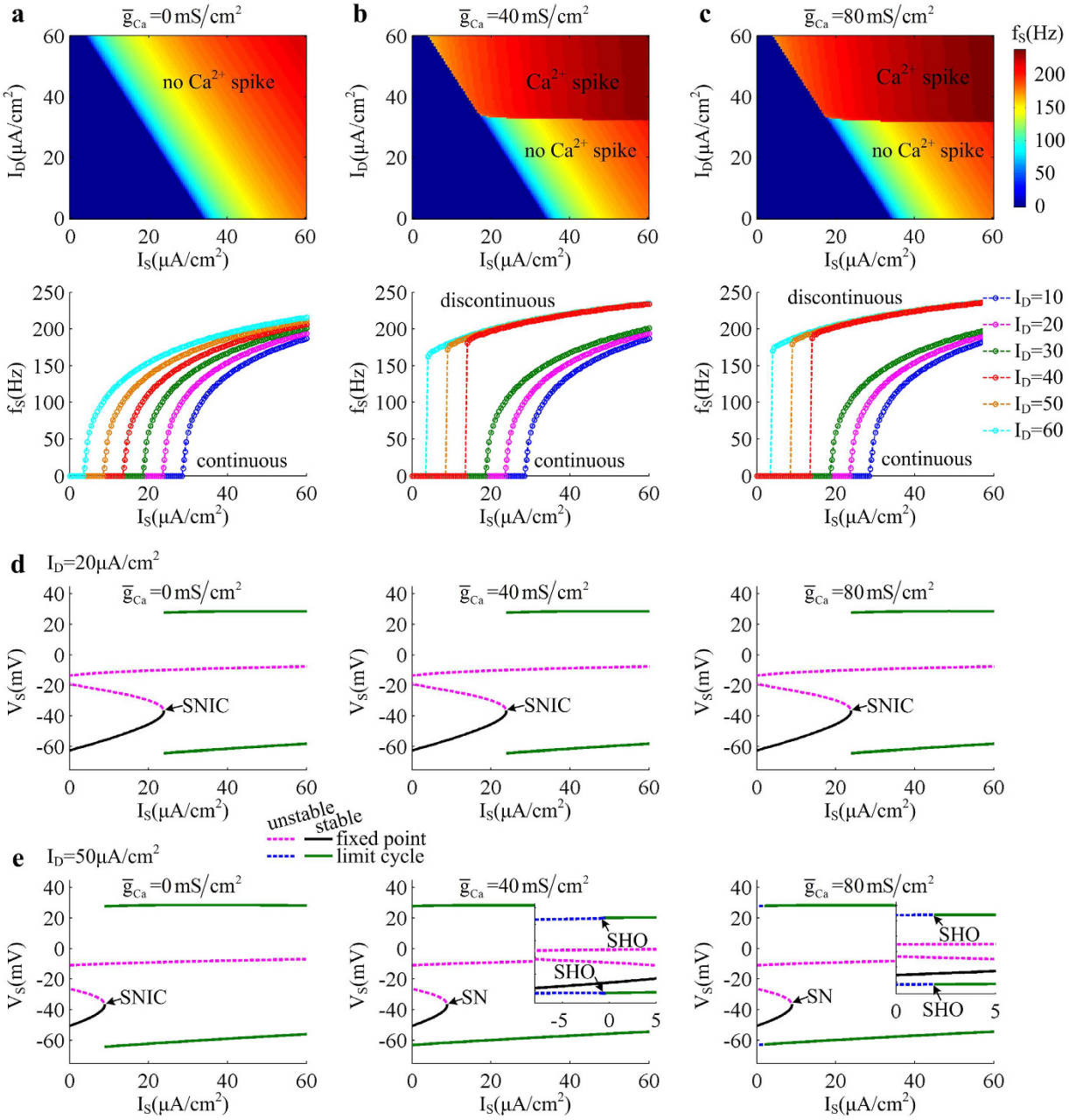

Figure 5. Firing properties evoked by coincident somatic and dendritic inputs. The firing rate f_S of the 5D model is calculated for three values of $\bar{g}_{Ca}$, which are **(a)** 0 mS/cm^2. **(b)** 40 mS/cm^2 and **(c)** 80 mS/cm^2, respectively. For **(a–c)**, top panels give the average firing rate f_S plotted against input I_S and I_D. Bottom panels show the $f_S - I_S$ curves with different values of I_D. The bifurcation diagrams related to coincident inputs at soma and dendrite with each value of $\bar{g}_{Ca}$ are given in **(d)** and **(e)**. Here the bifurcation parameter is somatic input I_S. We compute one-parameter bifurcation with two values of dendritic input, which are **(d)** $I_D = 20$ μA/cm^2 and **(e)** 50 μA/cm^2. The lower value of I_D is unable to activate dendritic Ca^{2+} conductance, but the latter could trigger dendritic Ca^{2+} spike. Type of the bifurcation for equilibrium or limit cycle is indicated on each plot.

spike initiating dynamics with $\bar{g}_{Ca}$ are due to dendritic Ca^{2+} activity, which endows dendrites with the powerful ability to actively integrate excitatory inputs.

Coincident somatic and dendritic inputs facilitate dendritic Ca^{2+} spike. Here we determine the firing properties of the 5D model neuron evoked by the stimulation of coincident I_S and I_D, which are summarized in (I_S, I_D) parameter space for $\bar{g}_{Ca} = 0$ mS/cm^2, 40 mS/cm^2 and 80 mS/cm^2. One can find that the threshold value of input I_S for triggering APs in somatic chamber decreases linearly with dendritic input I_D (Fig. 5a–c). This

is because that introducing positive I_D results in a depolarizing current transmitted to somatic chamber. Such current increases the level of neuronal excitability and makes it more prone to generate APs to somatic stimulus. Then, the rheobase of I_S decreases with dendritic input I_D.

Varying Ca^{2+} conductance $\bar{g}_{Ca}$ produces no effects on the rheobase of I_S in the observed range of I_D, which only determines whether there is dendritic Ca^{2+} spike. When blocking Ca^{2+} current (i.e., $\bar{g}_{Ca} = 0\ mS/cm^2$), the dendrite is passive and there is no dendritic Ca^{2+} spike in (I_S, I_D) parameter space. Here the f_S–I_S curve is always continuous in the range of $0 \le I_D \le 60\ \mu A/cm^2$ (Fig. 5a), which is generated by a SNIC bifurcation of equilibrium (Fig. 5d). With $\bar{g}_{Ca} = 40\ mS/cm^2$ or $80\ mS/cm^2$, there is dendritic Ca^{2+} spike elicited in (I_S, I_D) parameter space once I_D reaches a threshold value. Such event causes firing rate f_S quickly to converge to its plateau level at the onset of I_S (Fig. 5b and c). Then, the $f_S - I_S$ curve becomes discontinuous, which is generated via a SN bifurcation of equilibrium (Fig. 5e). Further, introducing dendritic Ca^{2+} current changes the bifurcation of limit cycle from SNIC to SHO, and makes it occur at another value of I_S below the bifurcation of equilibrium. Meanwhile, increasing $\bar{g}_{Ca}$ is also able to alter the value of I_S for causing the SHO bifurcation of limit cycle (Fig. 5e).

We also find that the threshold values of apical input I_D for evoking dendritic Ca^{2+} spike in (I_S, I_D) parameter space are significantly lower than those in the absent of I_S. This indicates that the bottom-up input is conducive to the initiation of dendritic Ca^{2+} spike. Particularly, with some moderate values of I_D, the Ca^{2+} current is unable to be activated by I_S above and close to the bifurcation point of equilibrium (Fig. 6a). Here only somatic input with sufficient intensity can force V_D to reach the threshold for initiating dendritic Ca^{2+} spike (Fig. 6b). It is known that the firing frequency f_S is an increasing function of I_S. Thus, the back-propagation of spiking behavior with high frequency contributes to activating Ca^{2+} spike, which is also referred to as BAC firing[17,23,26]. These results demonstrate that the dendritic Ca^{2+} spike is the outcome of the interaction between back-propagated APs and excitatory synaptic inputs (Fig. 6c). Such prolonged regenerative spikes elicited in apical dendrites can be forward propagated to the AP initiation zone to modulate the final output of the neuron.

Discussion

Our simulations have shown that injecting current to soma alone makes the 5D model neuron generate continuous input-output relation through a SNIC bifurcation of equilibrium. Here the bottom-up input from soma to dendrite is unable to activate dendritic Ca^{2+} conductance. Thus, varying Ca^{2+} conductance produces no effects on the output APs. Injecting current to apical dendrite alone results in a distinct input-output relation. When blocking Ca^{2+} channel, the input-output relation is still continuous, and the bifurcation structures of equilibrium and limit cycle both remain the same. When there is active Ca^{2+} channel in dendrite, the apical input with sufficient intensity is able to activate Ca^{2+} conductance and trigger a prolonged Ca^{2+} spike. This event boosts depolarized input as it spreads to soma, and facilitates the initiation of somatic APs. Under this condition, the neuron generates a burst of high-frequency APs during the course of dendritic Ca^{2+} spike. Then, the $f_S - I_D$ curve becomes discontinuous, and the firing rate quickly reaches a plateau level. These simulations demonstrate that the top-down information received by passive or active dendrite modulates the output APs in a distinct way, which depends critically on the site of synaptic inputs.

The firing rate of the 5D model neuron evoked by conjunct inputs to dendrite and soma is summarized in (I_S, I_D) parameter space. It is shown that simultaneously injecting constant current to two chambers shifts the threshold of $f_S - I_S$ curve to a lower value. When blocking dendritic Ca^{2+} current, the top-down input arriving at apical dendrite only increases the excitability of the neuron and reduces the rheobase of somatic input, which does not alter the shape of input-output relation. For the dendrite with Ca^{2+} channel, the top-down input with sufficient intensity triggers Ca^{2+} spike. This event results in a burst of APs in soma and significantly increases firing frequency, which leads to a discontinuous input-output relation. Here the timing of burst is able to detect whether there are coincident somatic and dendritic inputs. In fact, such burst pattern associated with dendritic Ca^{2+} spike has been observed in previous experimental[26,30–32] and modeling[35,37,39,40] reports. We have not only reproduced it with a simplified conductance-based model, but also determined the dynamical basis of relevant spike initiation with phase plane analysis. These investigations could contribute to uncovering how the Ca^{2+} activity in apical dendrites participates in neuronal computation.

It is shown that somatic input decreases the threshold value of apical input for triggering dendritic spike. This indicates that the back-propagating APs are conducive to the initiation of dendritic Ca^{2+} spike, i.e., BAC firing occurs. The simulations with our simple 5D model suggest that the generation of BAC firing arises from the interactions between back-propagating spikes and dendritic excitatory input, which is in accordance with previous predictions[17,23,26,27]. During this procedure, the back-propagating APs play a crucial role in connecting two zones of spike initiation, which enables the integration of synaptic inputs to be disturbed in space and time. Meanwhile, BAC firing is a common mechanism for pyramidal neuron to associate conjunct somatic and dendritic inputs[25]. Without BAC firing, the dendritic input has much less effects on the firing behavior than somatic input. Once it occurs, the firing rate and spike timing is dominated by the input received by apical dendrites. Thus, this event completely alters the relative importance of synaptic inputs to the cell. Two-compartment model is the minimum individual unit of the neuron to capture such complex phenomenon. Each chamber has its own mechanism for spike initiation, which enables the neuron to integrate synaptic inputs simultaneously in two separated regions. Thus, it can effectively reproduce the BAC firing. Further, earlier *in vitro* experiment[26] has predicted that the distal dendritic inputs lead to a higher gain and higher variability of the spike train than somatic input. This phenomenon is missing in our simulations, which is because that the injected currents here are all deterministic and do not include noise. Larkum *et al.*[26] have shown that the noisy components in current injection are the dominant factor for relevant gain modulation, since they significantly alter the initial slope of input-output relation.

The dendritic Ca^{2+} spikes in our simulations are triggered by current steps injected to the dendrite. Its roles are discussed in augmenting the influence of dendritic current flowing from the dendrite to the soma over the

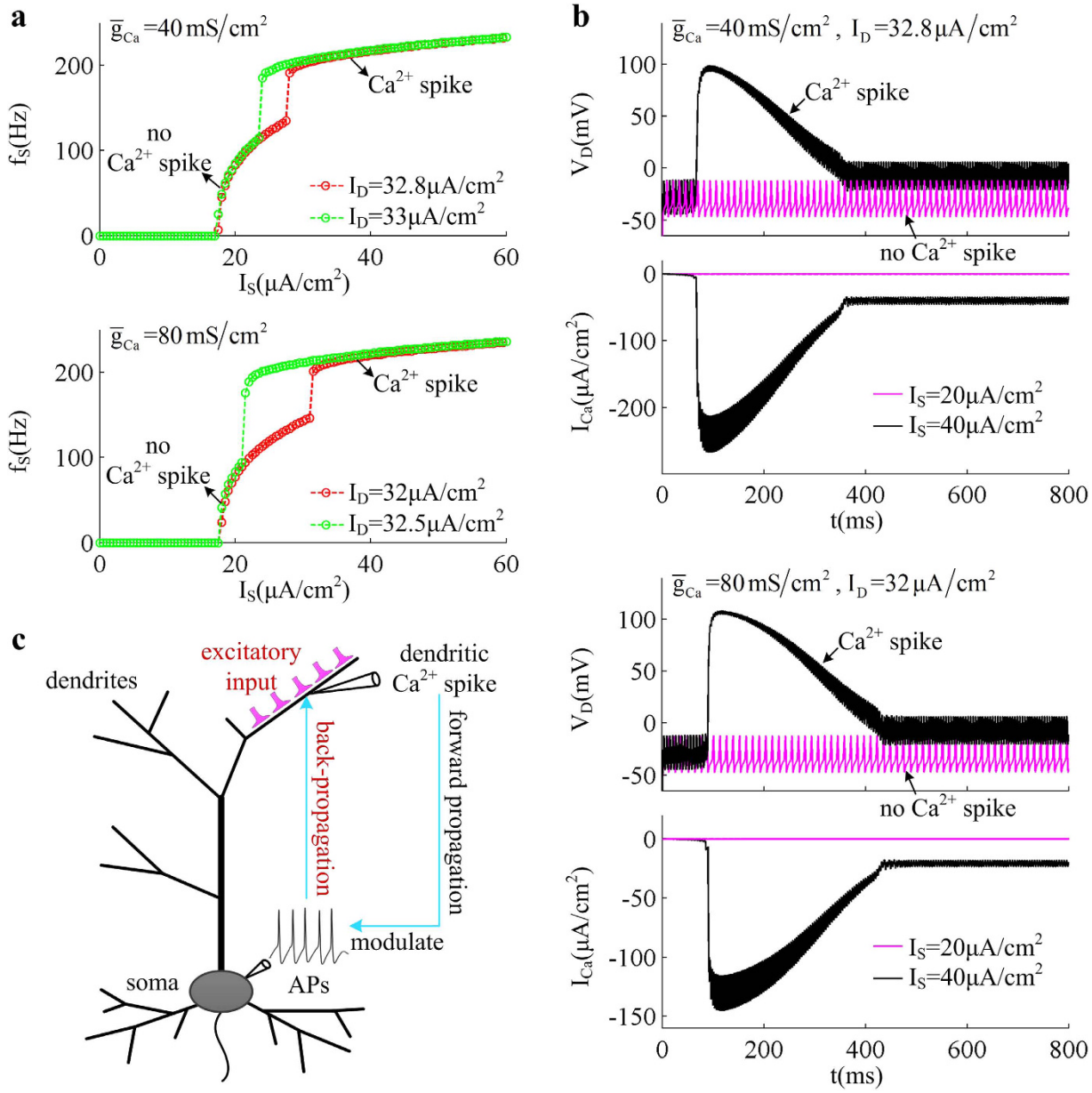

Figure 6. BAC firing evoked by coincident injections to two chambers. (**a**) $f_S - I_S$ curves of 5D model with $\bar{g}_{Ca}$ = 40 mS/cm^2 and 80 mS/cm^2. For $\bar{g}_{Ca}$ = 40 mS/cm^2, the value of dendritic input is I_D = 32.8 μA/cm^2 and 33 μA/cm^2. For $\bar{g}_{Ca}$ = 80 mS/cm^2, they are I_D = 32 μA/cm^2 and 32.5 μA/cm^2. (**b**) Dendritic voltage V_D and associated Ca^{2+} current I_{Ca} for each value of $\bar{g}_{Ca}$. The value of I_S and I_D are indicated in each plot. (**c**) Dendritic Ca^{2+} spike is evoked by the interactions between the back-propagating APs and the excitatory inputs received by apical dendrites. The Ca^{2+} spike induced by back-propagating APs is also referred to as BAC firing, which can be propagated to soma to modulate the output APs.

Na$^+$-APs. That is, the influences of relevant Ca^{2+} spike are studied in the presence of background activity. This makes the argument that Ca^{2+} spike augments dendritic current problematic. To determine how dendritic Ca^{2+} spike influences somatic APs by itself, we use apical input to generate a brief pulse to trigger a single dendritic Ca^{2+} spike and repeat above simulations. As expected, the inward current associated with dendritic Ca^{2+} spike provides a strong local depolarization that boosts apical input. The resulting sustained depolarization spreads to the soma and causes a burst of high-frequency APs (Fig. 7). These modulatory effects are similar to that evoked by current steps. It indicates that a Ca^{2+} spike in apical dendrites without additional dendritic input influences the initiation of somatic APs just the same as those with dendritic inputs.

Many Ca^{2+}-models include the dynamics of intracellular Ca^{2+} concentration $[Ca]$[37–39,43,49–53], which is tightly related to the Ca^{2+} influx through voltage-gated channels. It has been used in modeling[37,39,40] and experimental[15,16] studies to characterize dendritic Ca^{2+} spike. Here we introduce the dynamics of $[Ca]$ and two types of Ca^{2+}-activated K$^+$ current to the dendrite of our 5D model (see Methods for model specification). By injecting

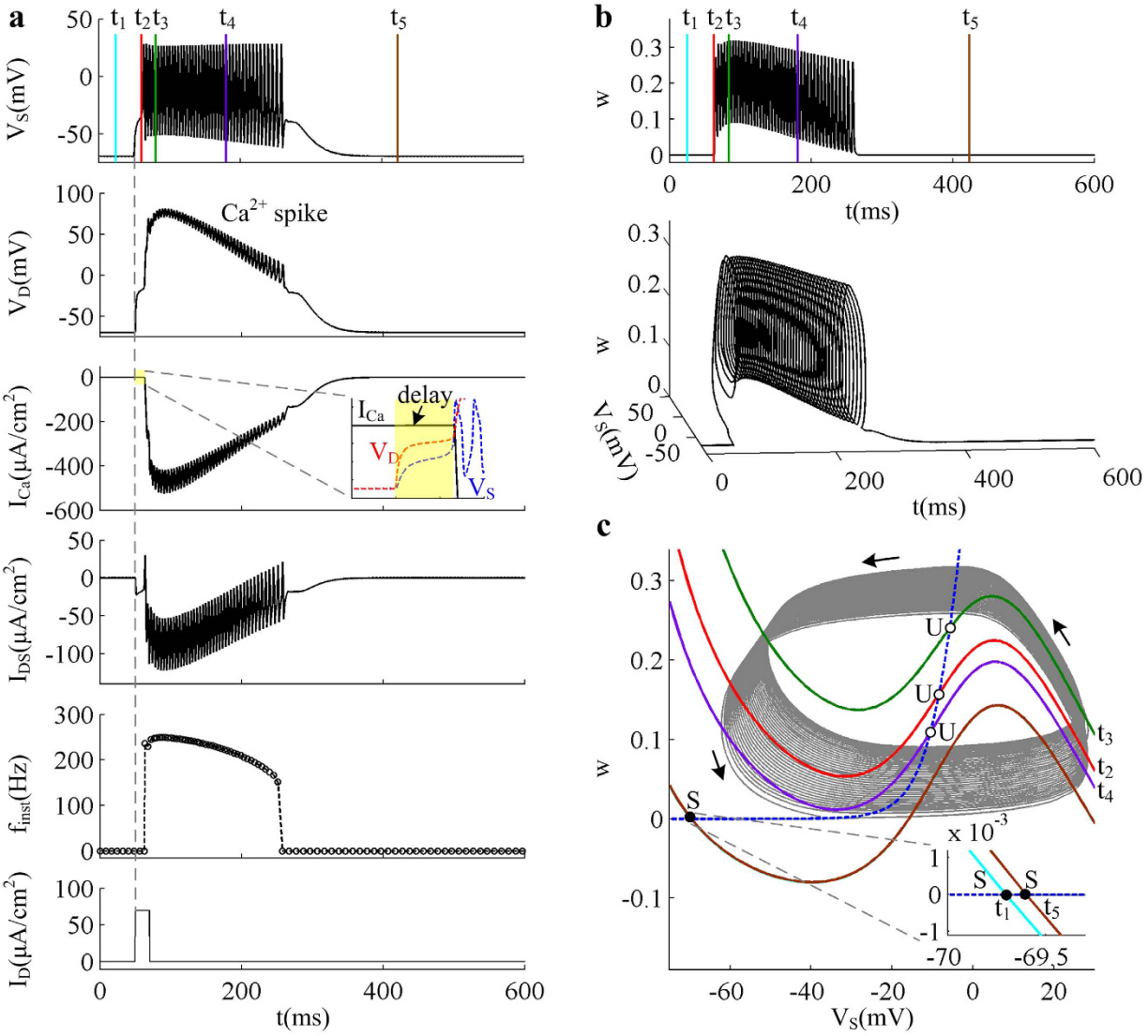

Figure 7. Somatic APs and initiating dynamics evoked by pulse injected at dendritic chamber. (**a**) Sample responses of the 5D model triggered by pulse input I_D in the cases of $\bar{g}_{Ca} = 20$ mS/cm^2. Somatic voltage V_S, dendritic voltage V_D, dendritic Ca^{2+} current I_{Ca}, internal current I_{DS}, and instantaneous firing rate f_{inst} are plotted against time. The amplitude of I_D is 70 μA/cm^2 and its duration is 20 ms. (**b**) Plot of K^+ activation variable w against time with $\bar{g}_{Ca} = 20$ mS/cm^2. The spike train recorded in soma is also plotted in $w - V_S - t$ space. Five color lines in panel (**a**) and (**b**) indicate the times at which the nullclines are calculated. (**c**) Two-dimensional phase portraits in $w - V_S$ plane. The V_S- and w-nullclines are respectively calculated at time point $t_1 - t_5$ indicated by colored lines in (**a**) and (**b**). Blue dotted line represents w-nullcline, and the inverted N-shape lines are the V_S-nullclines at corresponding time point. Gray solid line is the V_S trajectory, and black arrows indicate its direction. 'S' indicates stable fixed point, and 'U' indicates unstable fixed point. Somatic injection is $I_S = 0$ μA/cm^2.

current step to apical dendrite, we repeat the simulations to test whether dendritic Ca^{2+} spike has effects comparable with those described above. It is shown that the neuron generates periodic bursting behavior to constant apical input after introducing Ca^{2+} concentration and K^+ currents (Fig. 8a), which makes the difference between burst and tonic spiking more distinguishable. As expected, each dendritic Ca^{2+} spike has similar effects on the initiation of somatic APs in more biophysically realistic model (Fig. 8) and in 5D model (Figs 2 and 7). This suggests that the simplifications inherent in our 5D two-compartment model do not compromise the applicability of our findings to biophysically realistic conditions.

As a common cell type in mammalian brain, pyramidal neurons have been studied with theoretical approaches that incorporate dendritic Ca^{2+} channel in multi-compartmental models[21,33–37]. These complex models may express more than 10 voltage-gated channels, which are non-homegenously distributed along the somato-dendritic axis. Using biophysically realistic, high-dimensional neuron models is reasonably straightforward. But they may fail to provide greater insights into the mechanism underlying AP initiation than the experiments upon which they are based, since they include so many extraneous details. There are also theoretical studies

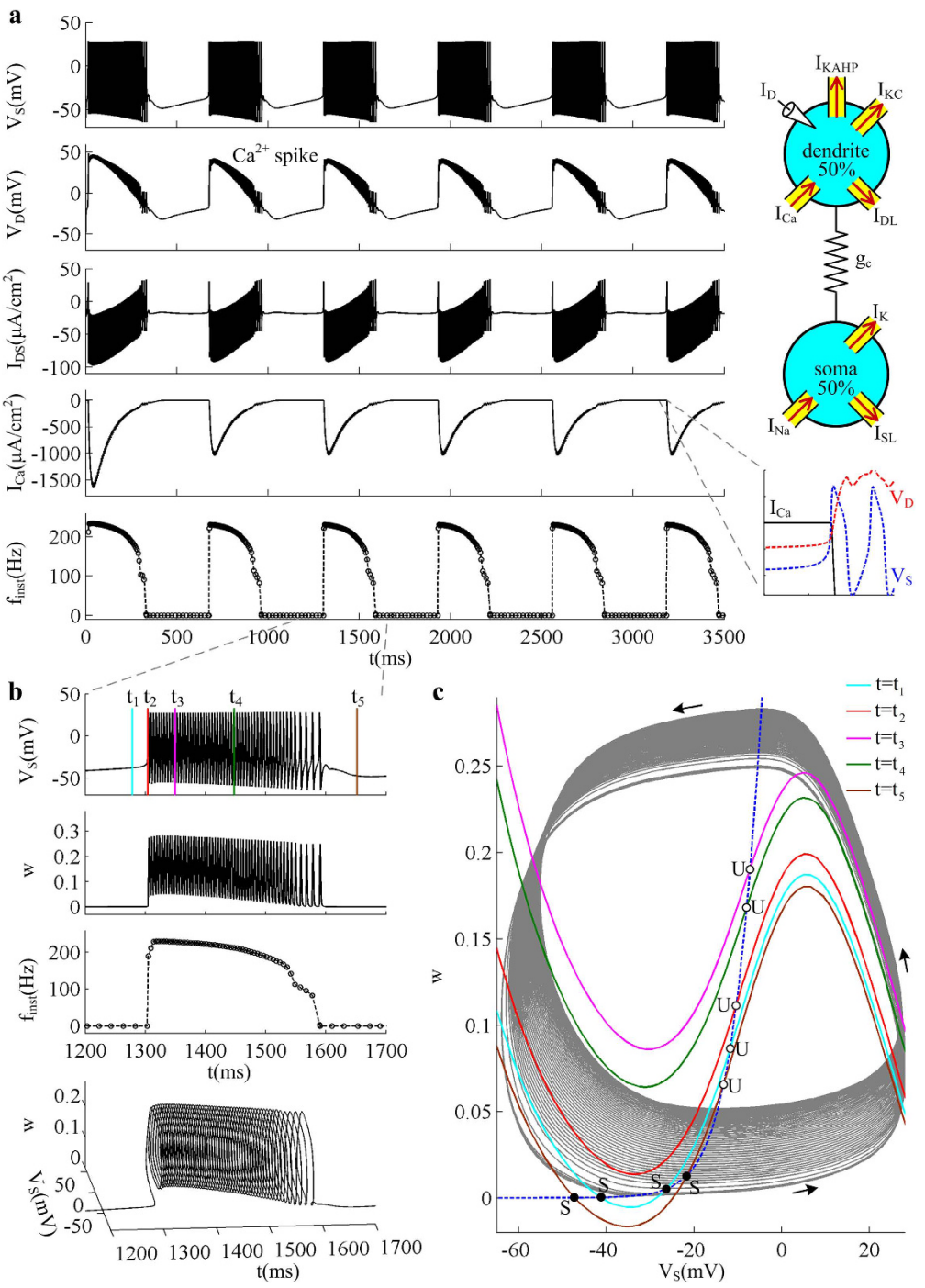

Figure 8. Bursting activities associated with dendritic Ca^{2+} spike in a more biophysically realistic model. (**a**) Schematic of the biophysically realistic model is shown in the top-right panel. The apical input is $I_D = 70\ \mu A/cm^2$, and somatic input is $I_S = 0\ \mu A/cm^2$. Left panels show the sample responses recorded in its soma. Somatic voltage V_S, dendritic voltage V_D, internal current I_{DS}, dendritic Ca^{2+} current I_{Ca}, and instantaneous firing rate f_{inst} are plotted against time. The bottom-right close-up shows that the Ca^{2+} conductance is activated when dendritic voltage V_D exceeds a threshold value. (**b**) Close-up of somatic voltage V_S, K^+ activation variable w, and firing rate f_{inst}. Bottom panel shows the close-up of V_S trajectory in $w - V_S - t$ space. Five color lines indicate the times at which the nullclines are calculated. (**c**) Two-dimensional phase portraits in $w - V_S$ plane. The V_S- and w-nullclines are respectively calculated at time point $t_1 - t_5$ indicated by colored lines in (**b**). Blue dotted line represents w-nullcline, and the inverted N-shape lines are the V_S-nullcline at corresponding time point. Gray solid line is the V_S trajectory, and black arrows indicate its direction. 'S' indicates stable fixed point, and 'U' indicates unstable fixed point. The maximum conductance of dendritic Ca^{2+} current is $\bar{g}_{Ca} = 40\ mS/cm^2$.

using simple two-compartment models to describe the Ca^{2+} activity of dendrites for pyramidal cell[38–43]. However, none of them has provided a satisfied interpretation of how dendritic Ca^{2+} spike participates in the initiating dynamics of somatic/axonal APs. Unlike earlier models, our model starts simple and excludes extraneous details, which is made only as complex as required to reproduce the phenomena of interest. It enables one to perform phase plane and bifurcation analysis on how Ca^{2+} spikes initiated in apical dendrites affect the global integration of the neuron. With our simple model, one can visualize and interpret how two-stage integration mode occurs in pyramidal cells. Even so, our predictions and corresponding interpretations require validation with complex models and experiments.

In summary, the current study addresses the importance of Ca^{2+} spike of apical dendrites in affecting the firing behaviors of two-compartment neurons during different sites of current injection. Our simulations provide a deep and interpretable insight into the connection between dendritic Ca^{2+} spike and firing pattern by relating them to somatic AP initiation. Determining how dendritic Ca^{2+} activities and input locations modulate the cellular responses is a pivotal first step toward uncovering how the Ca^{2+} activity of active dendrite participates in neuronal computation. The simplified two-compartment model proposed here is able to capture the complex phenomena of pyramidal neurons in experiments, which could be used to obtain a mechanistic understanding about how relevant circuits participate in cortical computation.

Methods

Simulations are based on the two-compartmental models of cortical pyramidal neuron, which are the reduced version of PR model. One compartment represents the apical dendritic zone, and the other one represents the basal integration zone around the soma plus axonal initial segment. From apical integration zone, the input signals transmitted to soma can be processed via dendritic Ca^{2+} spike. Two-compartment neuron is the simplest structure to capture such spatial inputs.

Our starting model is derived by introducing a voltage-dependent Ca^{2+} current to the passive dendrite of a simple two-compartment model proposed in our earlier studies[45,46]. The right panel of Fig. 1a shows the schematic representation of the two-compartment neuron, which is a 5D model. There are three ionic currents in somatic compartment, which are inward Na^+ current (I_{Na}), outward K^+ current (I_k), and passive leak current (I_{SL}). Here two active currents, i.e., I_{Na} and I_k, are responsible for generating APs. For dendritic chamber, there are two ionic currents, which are inward Ca^{2+} current (I_{Ca}) and passive leak current (I_{DL}). The somatic and dendritic chambers are connected by an internal coupling conductance $g_c = 1\ mS/cm^2$. The dynamics of their membrane potential V_S and V_D are governed by the following current-balance equations

$$\begin{aligned} C_m \frac{dV_S}{dt} &= \frac{I_S}{p} + \frac{I_{DS}}{p} - I_{Na} - I_K - I_{SL} \\ C_m \frac{dV_D}{dt} &= \frac{I_D}{1-p} - \frac{I_{DS}}{1-p} - I_{Ca} - I_{DL} \end{aligned} \tag{1}$$

where $C_m = 2\ \mu F/cm^2$ is the membrane capacitance, p = somatic area/total area $= 0.5$ is a morphological parameter. $I_{DS} = g_c(V_D - V_S)$ is the internal current that flows through conductance g_c and connects two chambers. I_S and I_D are two input currents respectively injected at soma and dendrite, which are used to stimulate the neuron.

Three voltage-dependent currents included in somatic chamber are

$$\begin{aligned} I_{Na} &= \bar{g}_{Na} m_\infty(V_S)(V_S - E_{Na}) \\ I_K &= \bar{g}_K w(V_S - E_K) \\ I_{SL} &= g_{SL}(V_S - E_{SL}) \end{aligned} \tag{2}$$

where $m_\infty(V_S) = 0.5\{1 + tanh[(V_S - \beta_m)/\gamma_m]\}$ is the steady-state activation function for inward Na^+ channel. w is the activation variable for slow K^+ current, which is governed by the following differential equation

$$\frac{dw}{dt} = \varphi_w \frac{w_\infty(V_S) - w}{\tau_w(V_S)} \tag{3}$$

Here $w_\infty(V_S) = 0.5\{1 + tanh[(V_S - \beta_w)/\gamma_w]\}$ and $\tau_w(V_S) = 1/\cosh[(V_S - \beta_w)/2\gamma_w]$ are respectively the steady-state activation function and time constant of this slow current. $\bar{g}_{Na} = 20\ mS/cm^2$, $\bar{g}_K = 20\ mS/cm^2$, $g_{SL} = 2\ mS/cm^2$ are the maximum conductances associated with the currents, and $E_{Na} = 50\ mV$, $E_K = -100\ mV$, $E_{SL} = -70\ mV$ are their relevant reversal potentials. Unless otherwise stated, $\beta_m = -1.2\ mV$, $\gamma_m = 18\ mV$, $\beta_w = 0\ mV$, $\gamma_w = 10\ mV$, and $\varphi_w = 0.15$.

Two voltage-dependent currents used in dendrite are

$$\begin{aligned} I_{Ca} &= \bar{g}_{Ca} nh(V_D - E_{Ca}) \\ I_{DL} &= g_{DL}(V_D - E_{DL}) \end{aligned} \tag{4}$$

where $g_{DL} = 2\ mS/cm^2$, $E_{DL} = -70mV$, $E_{Ca} = 120mV$, and Ca^{2+} maximum conductance $\bar{g}_{Ca}$ is varied as explained in Results. The dynamics of Ca^{2+} current is governed by an activation variable n and an inactivation variable h, which are characterized by the following equations

$$\frac{dn}{dt} = \frac{n_\infty(V_D) - n}{\tau_n}$$
$$\frac{dh}{dt} = \frac{h_\infty(V_D) - h}{\tau_h} \quad (5)$$

$\tau_n = 15$ ms and $\tau_h = 80$ ms are the time constant of the first-order kinetics for variable n and h. Their steady-state functions are

$$n_\infty(V_D) = \frac{1}{1 + \exp[-(V_D + 9)/0.5]}$$
$$h_\infty(V_D) = \frac{1}{1 + \exp[(V_D + 21)/0.5]} \quad (6)$$

The kinetics of dendritic Ca^{2+} channel here is the same as that described by Larkum *et al.*[26]. Unless otherwise stated, our stimulations are all based on this 5D model.

To make above 5D two-compartment model more biophysically realistic, we introduce the dynamics of intracellular Ca^{2+} concentration $[Ca]$ and two types of Ca^{2+}-activated K^+ current to its dendrite (see Fig. 8). The K^+ channels include short-duration Ca^{2+}-dependent K^+ current (I_{KC}) and long-duration Ca^{2+}-dependent K^+ current (I_{KAHP}), which are commonly distributed in the dendrites of pyramidal cells[37,39,40]. Their activations are both related to the dynamics of $[Ca]$. After introducing I_{KC} and I_{KAHP}, the membrane equation for dendritic voltage V_D becomes

$$C_m\frac{dV_D}{dt} = \frac{I_D}{1-p} - \frac{I_{DS}}{1-p} - I_{Ca} - I_{KC} - I_{KAHP} - I_{DL} \quad (7)$$

The details of I_{KC} and I_{KAHP} follow the descriptions by Pinsky and Rinzel[39], which are $I_{KC} = \bar{g}_{KC} c\chi([Ca])(V_D - E_K)$, and $I_{KAHP} = \bar{g}_{KAHP} q(V_D - E_K)$. Values of the maximum conductance are $\bar{g}_{KC} = 15$ mS/cm^2 and $\bar{g}_{KAHP} = 0.8$ mS/cm^2. The kinetics of their activation variable c and q obeys

$$\frac{dc}{dt} = \frac{c_\infty(V_D) - c}{\tau_c} = \alpha_c(1 - c) - \beta_c c$$
$$\frac{dq}{dt} = \frac{q_\infty(V_D) - q}{\tau_q} = \alpha_q(1 - q) - \beta_q q \quad (8)$$

where

$$\alpha_c = \begin{cases} \dfrac{\exp\left[\left(\frac{V_D - 10}{11}\right) - \left(\frac{V_D - 6.5}{27}\right)\right]}{18.975} & (V_D \le 50\text{mV}) \\ 2\exp\left[\left(\dfrac{6.5 - V_D}{27}\right)\right] & (V_D > 50\text{mV}) \end{cases}$$

$$\beta_c = \begin{cases} 2\exp\left(\dfrac{6.5 - V_D}{27}\right) - \alpha_c & (V_D \le 50\text{mV}) \\ 0 & (V_D > 50\text{mV}) \end{cases} \quad (9)$$

$$\alpha_q = \min(0.00002[Ca], 0.01),\ \beta_q = 0.001$$
$$\chi([Ca]) = \min([Ca]/250, 1)$$

The kinetics for intracellular Ca^{2+} concentration $[Ca]$ follows

$$\frac{d[Ca]}{dt} = -0.13 I_{Ca} - 0.075[Ca] \quad (10)$$

That is, the $[Ca]$ is increased proportionally to Ca^{2+} influx I_{Ca}[37,39]. All other parameters in this more biophysically realistic model are the same as in the 5D model.

Note that the dynamics of $[Ca]$ is not considered in the simple 5D model. As mentioned in Introduction, dendritic Ca^{2+} spike is the voltage transient caused by the activation of dendritic Ca^{2+} conductance[5–7,11,23]. It is a local regenerative response involving the positive feedback loop between dendritic voltage and Ca^{2+} influx[6,7]. Using a voltage-dependent current I_{Ca} is sufficient to reproduce such regenerative dendritic response and its dependence on Ca^{2+} dynamics[26]. By excluding the extraneous details, we propose a biophysical model complex enough to reproduce dendritic Ca^{2+} spike yet simple enough for characterizing its effects on the initiating dynamics of somatic APs. Further, the results in Fig. 8 show that ignoring the dynamics of Ca^{2+} concentration $[Ca]$ does not alter our predictions about how dendritic spike affects the initiating dynamics of somatic APs.

Finally, the two-compartment models are integrated in MATLAB using numerical integrator ode23, with a time resolution of 0.01 ms. The phase plane and bifurcation analyses are performed with the publicly available software package XPPAUT[54].

References

1. Spruston, N. Pyramidal neurons: dendritic structure and synaptic integration. *Nat. Rev. Neurosci.* **9,** 206–221 (2008).
2. Elston, G. N. Cortex, cognition and the cell: new insights into the pyramidal neuron and prefrontal function. *Cereb. Cortex* **13,** 1124–1138 (2003).
3. Ramon y Cajal, S. *Histology of the nervous system of man and vertebrates* (Oxford University Press, Oxford, 1995).
4. Palmer, L. M. Dendritic integration in pyramidal neurons during network activity and disease. *Brain Res. Bull.* **103,** 2–10 (2014).
5. Grienberger, C., Chen, X. & Konnerth, A. Dendritic function *in vivo*. *Trends Neurosci.* **38,** 45–54 (2015).
6. Stuart, G. J. & Spruston, N. Dendritic integration: 60 years of progress. *Nat. Neurosci.* **18,** 1713–21 (2015).
7. Major, G., Larkum, M. E. & Schiller, J. Active properties of neocortical pyramidal neuron dendrites. *Annu. Rev. Neurosci.* **36,** 1–24 (2013).
8. Branco, T. & Häusser, M. The single dendritic branch as a fundamental functional unit in the nervous system. *Curr. Opin. Neurobiol.* **20,** 494–502 (2010).
9. Branco, T. & Häusser, M. Synaptic integration gradients in single cortical pyramidal cell dendrites. *Neuron*. **69,** 885–92 (2011).
10. Vetter, P., Roth, A. & Häusser, M. Propagation of action potentials in dendrites depends on dendritic morphology. *J. Neurophysiol.* **85,** 926–37 (2001).
11. Tran-Van-Minh, A. *et al.* Contribution of sublinear and supralinear dendritic integration to neuronal computations. *Front. Cell. Neurosci*. **9,** 67 (2015).
12. Kitamura, K. & Häusser, M. Dendritic calcium signaling triggered by spontaneous and sensory-evoked climbing fiber input to cerebellar Purkinje cells *in vivo*. *J. Neurosci.* **31,** 10847–58 (2011).
13. Branco, T., Clark, B. A. & Häusser, M. Dendritic discrimination of temporal input sequences in cortical neurons. *Science* **329,** 1671–5 (2010).
14. Larkum, M. E. & Nevian, T. Synaptic clustering by dendritic signalling mechanisms. *Curr. Opin. Neurobiol.* **18,** 321–331 (2008).
15. Schiller, J., Schiller, Y., Stuart, G. & Sakmann, B. Calcium action potentials restricted to distal apical dendrites of rat neocortical pyramidal neurons. *J. Physiol.* **505,** 605–616 (1997).
16. Larkum, M. E., Kaiser, K. M. M. & Sakmann, B. Calcium electrogenesis in distal apical dendrites of layer 5 pyramidal cells at a critical frequency of back-propagating action potentials. *Proc. Natl. Acad. Sci. USA* **96,** 14600–14604 (1999).
17. Larkum, M. E., Zhu, J. J. & Sakmann, B. A new cellular mechanism for coupling inputs arriving at different cortical layers. *Nature* **398,** 338–341 (1999).
18. Katz, Y. *et al.* Synapse distribution suggests a two-stage model of dendritic integration in CA1 pyramidal neurons. *Neuron* **63,** 171–7 (2009).
19. Gasparini, S. & Magee, J. C. State-dependent dendritic computation in hippocampal CA1 pyramidal neurons. *J. Neurosci.* **26,** 2088–2100 (2006).
20. Gasparini, S., Migliore, M. & Magee, J. C. On the initiation and propagation of dendritic spikes in CA1 pyramidal neurons. *J. Neurosci.* **24,** 11046–11056 (2004).
21. Chua, Y. & Morrison, A. Effects of calcium spikes in the layer 5 pyramidal neuron on coincidence detection and activity propagation. *Front. Comput. Neurosci*. **10,** 76 (2016).
22. Shai, A., Anastassiou, C., Larkum, M. & Koch, C. Physiology of layer 5 pyramidal neurons in mouse primary visual cortex: coincidence detection through bursting. *PLoS Comput. Biol.* **11,** e1004090 (2015).
23. Larkum, M. A cellular mechanism for cortical associations: an organizing principle for the cerebral cortex. *Trends Neurosci.* **36,** 141–151 (2013).
24. Grienberger, C., Chen, X. & Konnerth, A. NMDA receptor-dependent multidendrite Ca2+ spikes required for hippocampal burst firing *in vivo*. *Neuron* **81,** 1274–81 (2014).
25. Larkum, M. E., Zhu, J. J. & Sakmann, B. Dendritic mechanisms underlying the coupling of the dendritic with the axonal action potential initiation zone of adult rat layer 5 pyramidal neurons. *J. Physiol.* **533,** 447–466 (2001).
26. Larkum, M. E., Senn, W. & Lüscher, H. R. Top-down dendritic input increases the gain of layer 5 pyramidal neurons. *Cereb. Cortex* **14,** 1059–1070 (2004).
27. Hage, T. A. & Khaliq, Z. M. Tonic firing rate controls dendritic Ca2+ signaling and synaptic gain in substantia nigra dopamine neurons. *J. Neurosci.* **35,** 5823–36 (2015).
28. Larkum, M. E., Nevian, T., Sandler, M., Polsky, A. & Schiller, J. Synaptic integration in tuft dendrites of layer 5 pyramidal neurons: a new unifying principle. *Science* **325,** 756–60 (2009).
29. Polsky, A., Mel, B. W. & Schiller, J. Computational subunits in thin dendrites of pyramidal cells. *Nat. Neurosci.* **7,** 621–627 (2004).
30. Palmer, L. M. *et al.* The cellular basis of GABA(B)-mediated interhemispheric inhibition. *Science* **335,** 989–93 (2012).
31. Larkum, M. E. & Zhu, J. J. Signaling of layer 1 and whisker evoked Ca2+ and Na+ action potentials in distal and terminal dendrites of rat neocortical pyramidal neurons *in vitro* and *in vivo*. *J. Neurosci.* **22,** 6991–7005 (2002).
32. Williams, S. R. & Stuart, G. J. Mechanisms and consequences of action potential burst firing in rat neocortical pyramidal neurons. *J. Physiol.* **521,** 467–482 (1999).
33. Hay, E. & Segev, I. Dendritic excitability and gain control in recurrent cortical microcircuits. *Cereb. Cortex* **25,** 3561–71 (2015).
34. Zomorrodi, R., Kröger, H. & Timofeev, I. Modeling thalamocortical cell: impact of Ca2+ channel distribution and cell geometry on firing pattern. *Front. Comput. Neurosci*. **2,** 5 (2008).
35. Siegel, M., Körding, K. P. & König, P. Integrating top-down and bottom-up sensory processing by somato-dendritic interactions. *J. Comput. Neurosci*. **8,** 161–73 (2000).
36. Miyasho, T. *et al.* Low-threshold potassium channels and a low-threshold calcium channel regulate Ca spike firing in the dendrites of cerebellar Purkinje neurons: a modeling study. *Brain Res.* **891,** 106–15 (2001).
37. Traub, R. D., Wong, R. K., Miles, R. & Michelson, H. A model of a CA3 hippocampal pyramidal neuron incorporating voltage-clamp data on intrinsic conductances. *J. Neurophysiol.* **66,** 635–50 (1991).
38. Ferguson, K. A. & Campbell, S. A. A two compartment model of a CA1 pyramidal neuron. *Canadian Applied Mathematics Quarterly* **17,** 293–307 (2009).
39. Pinsky, P. F. & Rinzel, J. Intrinsic and network rhythmogenesis in a reduced Traub model for CA3 neurons. *J. Comput. Neurosci*. **1,** 39–60 (1994).
40. Mainen, Z. F. & Sejnowski, T. J. Influence of dendritic structure on firing pattern in model neocortical neurons. *Nature* **382,** 363–6 (1996).
41. Naud, R., Bathellier, B. & Gerstner, W. Spike-timing prediction in cortical neurons with active dendrites. *Front. Comput. Neurosci*. **8,** 90 (2014).
42. Ilan, L. B., Gidon, A. & Segev, I. Interregional synaptic competition in neurons with multiple STDP-inducing signals. *J. Neurophysiol.* **105,** 989–98 (2011).
43. Wang, X. J. Calcium coding and adaptive temporal computation in cortical pyramidal neurons. *J. Neurophysiol.* **79,** 1549–66 (1998).

44. Brette, R. What is the most realistic single-compartment model of spike initiation? *PLoS Comput. Biol.* **11,** e1004114 (2015).
45. Yi, G. S. *et al.* Exploring how extracellular electric field modulates neuron activity through dynamical analysis of a two-compartment neuron model. *J. Comput. Neurosci.* **36,** 383–99 (2014).
46. Yi, G. S. *et al.* Neuronal spike initiation modulated by extracellular electric fields. *PLoS One* **9,** e97481 (2014).
47. Yi, G. S. *et al.* Spike-frequency adaptation of a two-compartment neuron modulated by extracellular electric fields. *Biol. Cybern.* **109,** 287–306 (2015).
48. Izhikevich, E. M. *Dynamical systems in neuroscience: the geometry of excitability and bursting* (The MIT Press, London, 2007).
49. Nadkarni, S. & Jung, P. Dressed neurons: modeling neural-glial interactions. *Phys. Biol.* **1,** 35–41 (2004).
50. Ma, J. & Tang, J. A review for dynamics of collective behaviors of network of neurons. *Sci. China Technol. Sci.* **58,** 2038–20045 (2015).
51. Goldberg, M., De Pittà, M., Volman, V., Berry, H. & Ben-Jacob, E. Nonlinear gap junctions enable long-distance propagation of pulsating calcium waves in astrocyte networks. *PLoS Comput. Biol.* **6,** e1000909 (2010).
52. Li, J. *et al.* Dynamic transition of neuronal firing induced by abnormal astrocytic glutamate oscillation. *Sci. Rep*. **6,** 32343 (2016).
53. Dayan, P. & Abbott, L. F. *Theoretical neuroscience: computational and mathematical modeling of neural systems* (The MIT Press, London, 2005).
54. Ermentrout, B. *Simulating, analyzing, and animating dynamical systems: a guide to Xppaut for researchers and students* (SIAM, Philadelphia, 2002).

Acknowledgements

This work was supported by grants from the National Natural Science Foundation of China (Nos. 61372010, 61471265 and 61601320), the China Postdoctoral Science Foundation (No. 2015M580202), and the Specialized Research Fund for the Doctoral Program of Higher Education (No. 20130032110065).

Author Contributions

G.S.Y., J.W. and X.L.W. conceived and designed the research, G.S.Y. and J.W. performed the simulations, G.S.Y., J.W. and X.L.W. wrote the paper. All authors reviewed the manuscript.

Additional Information

Competing Interests: The authors declare no competing financial interests.

How to cite this article: Yi, G. *et al.* Action potential initiation in a two-compartment model of pyramidal neuron mediated by dendritic Ca^{2+} spike. *Sci. Rep.* **7**, 45684; doi: 10.1038/srep45684 (2017).

Publisher's note: Springer Nature remains neutral with regard to jurisdictional claims in published maps and institutional affiliations.